

# Zero-Shot Denoising of Distributed Acoustic Sensing Data using Deep Priors

Jannik Mänzer

Bachelor of Science  
March 2025

Supervisors:

Prof. Dr. Stefan Harmeling  
Sebastian Konietzny

Artificial Intelligence (VIII)

Department of Computer Science  
TU Dortmund University



# Abstract

Lorem ipsum dolor sit amet, consetetur sadipscing elitr, sed diam nonumy eirmod tempor invidunt ut labore et dolore magna aliquyam erat, sed diam voluptua. At vero eos et accusam et justo duo dolores et ea rebum. Stet clita kasd gubergren, no sea takimata sanctus est Lorem ipsum dolor sit amet. Lorem ipsum dolor sit amet, consetetur sadipscing elitr, sed diam nonumy eirmod tempor invidunt ut labore et dolore magna aliquyam erat, sed diam voluptua. At vero eos et accusam et justo duo dolores et ea rebum. Stet clita kasd gubergren, no sea takimata sanctus est Lorem ipsum dolor sit amet.



# Contents

<b>1</b>	<b>Introduction</b>	<b>1</b>
<b>2</b>	<b>Background</b>	<b>3</b>
2.1	Denoising . . . . .	3
2.2	Distributed Acoustic Sensing . . . . .	3
2.3	Deep Learning . . . . .	5
2.3.1	Deep Neural Networks . . . . .	5
2.3.2	Convolutional Neural Networks . . . . .	6
2.3.3	Normalization . . . . .	6
2.3.4	Attention Mechanisms . . . . .	7
2.4	Fourier Transform . . . . .	7
<b>3</b>	<b>Related Work</b>	<b>9</b>
3.1	Supervised Methods . . . . .	9
3.2	Self-Supervised Methods . . . . .	10
3.2.1	N2N-Based Methods . . . . .	10
3.2.2	Blind-Spot-Based Methods . . . . .	11
<b>4</b>	<b>Methods</b>	<b>13</b>
4.1	Deep Image Prior . . . . .	13
4.1.1	Early Stopping . . . . .	15
4.1.2	Total Variation . . . . .	16
4.2	Deep Diffusion Image Prior . . . . .	16
4.3	Self-Guided Deep Image Prior . . . . .	16
<b>5</b>	<b>Results</b>	<b>17</b>
<b>6</b>	<b>Discussion</b>	<b>19</b>
<b>7</b>	<b>Conclusion</b>	<b>21</b>
	<b>Bibliography</b>	<b>22</b>

<b>A</b>	<b>Supplementary Information</b>	<b>27</b>
A.1	Acronyms . . . . .	27

# Chapter 1

## Introduction

Lorem ipsum dolor sit amet, consetetur sadipscing elitr, sed diam nonumy eirmod tempor invidunt ut labore et dolore magna aliquyam erat, sed diam voluptua. At vero eos et accusam et justo duo dolores et ea rebum. Stet clita kasd gubergren, no sea takimata sanctus est Lorem ipsum dolor sit amet. Lorem ipsum dolor sit amet, consetetur sadipscing elitr, sed diam nonumy eirmod tempor invidunt ut labore et dolore magna aliquyam erat, sed diam voluptua. At vero eos et accusam et justo duo dolores et ea rebum. Stet clita kasd gubergren, no sea takimata sanctus est Lorem ipsum dolor sit amet.





## Chapter 2

# Background

This chapter provides the necessary background for the denoising methods explored in this work. We begin by defining the general denoising problem and discussing its inherent challenges. We then introduce distributed acoustic sensing (DAS) as a real-world application and highlight the unique difficulties it poses. Finally, we present key deep learning concepts and techniques that are used in the context of denoising.

### 2.1 Denoising

In general, denoising refers to the process of recovering a clean signal from a noisy observation. Formally, this is described by the inverse problem

$$y = x + n \tag{2.1}$$

where  $y$  is the noisy observation,  $x$  is the underlying clean signal and  $n$  represents some form of noise, for example Gaussian noise  $n \sim \mathcal{N}(\mathbf{0}, \sigma^2 \mathbf{I})$ . Since both the noise and its distribution are often unknown, denoising is an inherently ill-posed problem, as multiple solutions can explain the same noisy data. Therefore, additional assumptions or constraints on the solution space are necessary, a process typically referred to as regularization. This can involve the use of a *prior*, which encodes our beliefs about the likely properties of the clean signal. The choice of regularizer or prior depends on the specific problem setting and the type of data involved.

### 2.2 Distributed Acoustic Sensing

Distributed acoustic sensing (DAS), also known as distributed vibration sensing (DVS) [6], is an innovative technology for high-resolution vibration measurements over large distances by utilizing fiber optic cables as sensor arrays. When a short laser pulse is sent through the fiber by a DAS interrogator unit, a fraction of the light is scattered back due to small variations or imperfections in the fiber. This phenomenon is referred to as Rayleigh scattering.

Vibrations along the cable caused by external influences, e.g., seismic events, strain the fiber, which in turn causes phase shifts in the backscattered light. These shifts are detected by the interrogator and, since the travel time of the light is known, can be used to accurately locate the strain along the cable [12]. In order to extract meaningful measurements, strain is analyzed over sections of the fiber, rather than at individual points. The length of these sections is called the gauge length, while another parameter, the channel spacing, determines how much this section is moved for each measurement, or channel, along the cable [4]. In practice, each channel corresponds to a virtual sensor capturing the average strain within its gauge length. Typically, the gauge length is selected to be bigger than the channel spacing, meaning that the measurement sections of neighboring channels overlap, as visualized in Figure 2.1. This concept of virtual sensors leads to high cost-effectiveness and, paired with the high sample rates enabled by the optical approach, allows measurements with significantly higher spatial and temporal resolution compared to conventional seismographs.

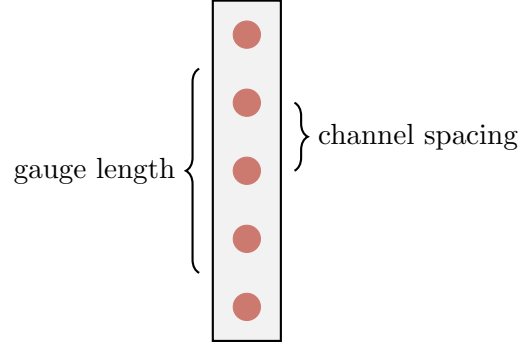


**Figure 2.1:** Gauge length and channel spacing. Red dots represent the individual channels along the fiber. Figure adapted from [4].

Despite these advantages, DAS systems often suffer from much lower signal quality than conventional seismographs, as they are more sensitive to various sources of noise. These can be divided into environmental noise and optical noise. Environmental noise includes natural phenomena such as winds or ocean waves, but also vibrations caused by vehicular

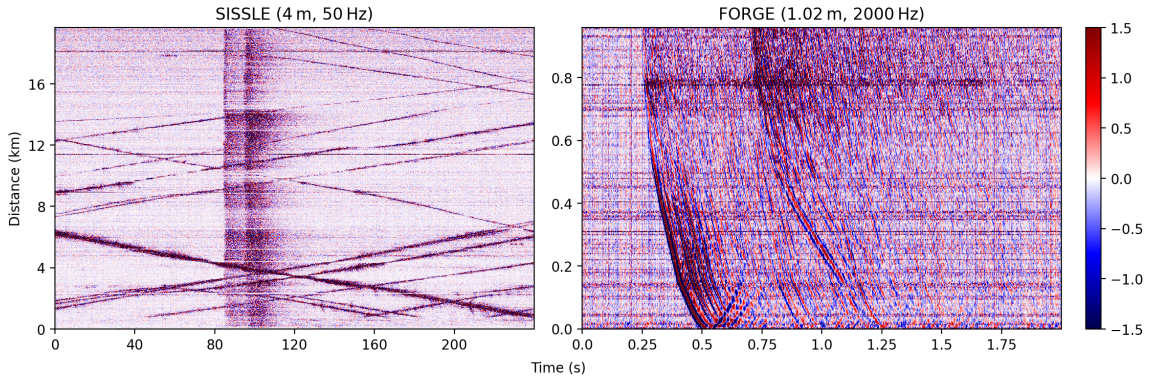


**Figure 2.2:** Types of noise in different DAS setups. Both measurements capture seismic activity; however, the SISSLE data mainly suffers from traffic noise (the diagonal lines). In contrast, erratic and common mode noise (the horizontal and vertical lines, respectively) are most prominent in the FORGE data.

and pedestrian traffic. Optical noise originates from various interactions between the light and the fiber. It includes high-amplitude erratic noise and common mode noise [3].

The actual noise characteristics of DAS data not only depend on the environment, but also the measurement parameters such as channel spacing and sample rate, as visualized in Figure 2.2 for data from the Sissle experiment near Haast, New Zealand [18] and the FORGE site in Utah [15].

## 2.3 Deep Learning

Deep learning is a subfield of machine learning that utilizes deep neural networks to learn complex patterns from data. Over the past decade, deep learning has established itself as the state-of-the-art approach for a wide range of problems across various different fields.

### 2.3.1 Deep Neural Networks

In its most basic form, a neural network consists of neurons organized in layers, where each neuron applies a linear transformation followed by a non-linear activation function. The output of a single neuron is given by

$$y = \varphi(\mathbf{w}^T \mathbf{x} + b) \quad (2.2)$$

for an input  $\mathbf{x} \in \mathbb{R}^n$ , a weight vector  $\mathbf{w} \in \mathbb{R}^n$ , a bias  $b \in \mathbb{R}$  and an activation function  $\varphi : \mathbb{R} \rightarrow \mathbb{R}$ . The outputs of each layer are then passed as inputs to the next layer, which is why this architecture is known as a fully-connected neural network. The activation functions are needed in order to avoid the network collapsing into a single linear transformation. Therefore, a neural network can be described as a function  $f_\theta : \mathcal{X} \rightarrow \mathcal{Y}$  parameterized by  $\theta$ , where  $\theta$  represents the weights and biases across all layers [5].

In order to optimize these parameters, a loss function  $L : \mathcal{Y} \times \mathcal{Y} \rightarrow \mathbb{R}$  is defined, which measures the difference between the predicted output and the target value. Now, the gradient of the loss function with respect to the parameters,  $\nabla_\theta L = \frac{\partial L}{\partial \theta}$ , represents the direction of steepest ascent. Therefore, by moving the parameters in the opposite direction of the gradient, the loss function can be minimized. Typically, the gradient is not calculated for a single data point or for the whole dataset, but instead for a small subset of the dataset, which is why this approach is referred to as (mini-batch) gradient descent. Backpropagation [22] is used to efficiently compute the gradient by making use of the chain rule, enabling fast optimization.

While traditionally neural networks only consisted of a few layers and required hand-crafted features to work effectively, advances in computing power allow modern architectures to automate feature extraction by using additional layers, hence the term *deep* neural network.

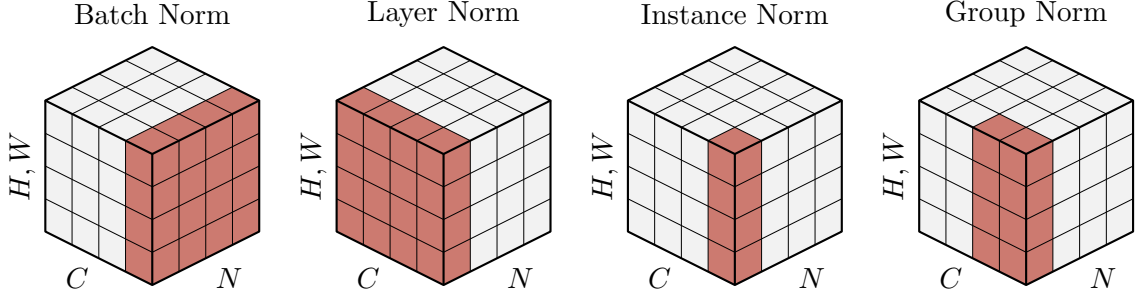


**Figure 2.3:** Different normalization techniques.  $N$  is the batch dimension,  $C$  is the channel dimension and  $H$  and  $W$  are the spatial dimensions of a 4D tensor. The input is normalized across the dimensions highlighted in red. Figure adapted from [29].

### 2.3.2 Convolutional Neural Networks

Convolutional neural networks (CNNs) [13] are a specific type of neural network that learns features using kernels. Prior to the rise of deep learning, such kernels were designed manually for various computer vision tasks, for example the Sobel kernel [23] used for edge detection. In CNNs, these kernels are automatically learned from data. In contrast to fully-connected layers, the output of a convolutional layer is obtained by convolution with one or multiple kernels, replacing the matrix multiplication. For a kernel  $\mathbf{K} \in \mathbb{R}^{n \times m}$ , the convolution is defined as

$$(\mathbf{X} * \mathbf{K})_{i,j} = \sum_{k=1}^n \sum_{l=1}^m X_{i+n,j+m} \cdot K_{k,l}. \quad (2.3)$$

The output of the convolution is then passed through a non-linear activation function, just like in fully-connected layers. CNNs provide two main advantages: First, since the weights are shared across the spatial dimensions, convolutional layers drastically reduce the number of parameters compared to fully-connected layers. Second, convolutions are translationally equivariant, meaning that local patterns in the input can be recognized regardless of their position, which makes CNNs very suitable for image data [5].

### 2.3.3 Normalization

During the training process, the inputs of each layer change with each iteration as the parameters are optimized. That slows down the training because now each layer has to adapt to the new distribution of its inputs. This process is often referred to as internal covariate shift. To counteract this issue, Ioffe et al. propose Batch Normalization (BN) [9]. The idea behind BN is to normalize the inputs across the whole mini-batch and their spatial dimensions. The normalized input for a channel  $i$  is given by

$$\hat{x}^{(i)} = \frac{x^{(i)} - \mu^{(i)}}{\sigma^{(i)}}, \quad (2.4)$$

where  $\mu^{(i)}$  and  $\sigma^{(i)}$  are the per-channel mean and standard deviation of the mini-batch, respectively. In order to allow the model to learn the identity if that were the optimal transformation, two additional learnable parameters,  $\gamma$  and  $\beta$ , are introduced. The output of the BN layer is then defined as

$$y^{(i)} = \gamma^{(i)} \hat{x}^{(i)} + \beta^{(i)}. \quad (2.5)$$

Since there are no batch statistics available at inference time, BN keeps track of the running mean and variance during training and uses these values for normalization. While BN is widely used, there exist various similar normalization techniques [1, 26, 29] mainly differing in the dimensions across which they are applied. A selection of them is visualized in Figure 2.3.

### 2.3.4 Attention Mechanisms

In neural networks, some input features are typically more important than others. An attention mechanism helps the network to focus on (*attend to*) the most relevant parts of the input, rather than processing all inputs equally. This works by dynamically reweighting the features based on their importance [20]. While attention is often associated with natural language processing (NLP), especially since the introduction of the Transformer architecture [27] where it is the underlying key principle, it also has applications beyond NLP. In computer vision, for example, it can help CNNs by reweighting feature channels [7] or highlighting important spatial regions.

## 2.4 Fourier Transform



## Chapter 3

# Related Work

In the last few years, deep-learning-based methods have been successfully applied to various image denoising tasks [24] and achieve state-of-the-art results. While these networks were traditionally trained in a supervised fashion, requiring clean target images, recent methods remove the dependency on clean data by leveraging self-supervision [31]. In this chapter, we give an overview of existing supervised and self-supervised approaches, presenting key principles and discussing their limitations.

### 3.1 Supervised Methods

Traditional supervised methods typically employ a neural network  $f_\theta$  to learn a mapping from a noisy image  $y$  to its clean counterpart  $x$ . Therefore, a dataset of paired clean and noisy images, denoted  $\{(y^i, x^i)\}_i^n$ , is essential for the training process. The corresponding optimization problem is given by

$$\operatorname{argmin}_{\theta} \sum_{i=1}^n \|f_\theta(y^i) - x^i\|_2^2. \quad (3.1)$$

Zhang et al. propose the denoising convolutional neural network (DnCNN) [32] which improves denoising performance by making use of residual learning, i.e., instead of directly predicting the clean image, it is trained to predict the noise in the noisy image. The denoised image is then obtained as  $\hat{x} = y - f_{\theta^*}(y)$  for trained parameters  $\theta^*$ . However, depending on the problem setting, acquiring the needed clean data can be difficult or even impossible, for example in medical imaging or also in DAS.

To address this issue, Lehtinen et al. propose Noise2Noise (N2N) [14], which does not require any clean data. Instead, it utilizes two independent noisy observations  $y_1 = x + n_1$  and  $y_2 = x + n_2$  of the same underlying clean signal  $x$  as input and target, respectively. The training objective then becomes

$$\operatorname{argmin}_{\theta} \sum_{i=1}^n \|f_\theta(y_1^i) - y_2^i\|_2^2. \quad (3.2)$$

This method relies on the assumption that the noise is zero-mean, i.e.,  $\mathbb{E}[n] = 0$ , which, due to linearity of expectation, implies that  $\mathbb{E}[y] = x$ . Since the MSE is a mean-seeking loss function, the network then learns to predict  $x$  implicitly. Given infinite data, the optimal solution is actually equivalent to the one obtained by training with clean targets. Although N2N is often impractical in practice because the required noisy-noisy pairs are difficult to obtain, it led to the development of other *self*-supervised approaches.

## 3.2 Self-Supervised Methods

Self-supervised methods are trained similarly to traditional supervised methods, but they do not rely on externally-provided target values. In the context of denoising, these approaches can be broadly categorized into two main strategies: N2N-based methods use a training objective similar to the one given by (3.2); however they generate their own noisy-noisy training pairs from individual noisy inputs. Blind-spot-based methods, on the other hand, exploit spatial correlations in the image using different masking strategies, either in the input or in the network architecture itself.

### 3.2.1 N2N-Based Methods

Noisier2Noise [19] builds upon N2N, but unlike N2N, it does not require a set of paired noisy-noisy images. Instead, it constructs these training pairs from individual noisy images only. Given a noisy input  $y$ , it generates an even noisier image  $z = y + m = x + n + m$ , with additional independent noise  $m$  following the same distribution as  $n$ . Once again, it is optimized through (3.2), using  $z$  as the input and  $y$  as the target. The authors argue that  $\mathbb{E}[y|z] = x + \frac{n+m}{2}$ , since  $\mathbb{E}[n] = \mathbb{E}[m]$ . Therefore, by the same reasoning as in N2N, given a sufficient amount of noisy images, the network should learn to predict the mean of  $x$  and  $z$ , which can then be used to obtain the denoised estimate as  $\hat{x} = 2f_{\theta^*}(z) - z$ . While this method removes the need for a paired dataset, it requires knowledge of the noise distribution in order to sample the additional noise.

Another approach based on N2N is Neighbor2Neighbor [8]. The key idea behind this method is to construct training pairs from the noisy input  $y$  by leveraging spatial redundancy through a sub-sampling strategy:  $y$  is divided into  $2 \times 2$  cells from each of which two neighboring pixels are randomly selected — one pixel is assigned to the first sub-sampled image and the other to the second. These sub-sampled images then build the noisy training pair. As a result of the sub-sampling, unlike in N2N, the underlying clean signal  $x$  is not exactly identical in the two noisy images. To address this, the authors extend the training strategy given by (3.2) by using an additional regularization term that encourages minimizing differences between sub-sampled versions of the denoised estimate.

Zero-Shot Noise2Noise [17] takes this idea one step further by enabling training on just one single noisy image instead of a set of noisy images. The term *zero-shot* refers to a



training setup where the model is supposed to make predictions for types of data it has never observed before without any training examples. This approach employs a similar sub-sampling strategy to obtain input and target values. In order to avoid overfitting to the noisy target, it makes use of residual learning, a symmetric loss and an additional regularization term enforcing consistency with respect to the order in which downsampling and inference are performed.

### 3.2.2 Blind-Spot-Based Methods

All blind-spot-based methods assume that noise is zero-mean and spatially independent, while the clean image signal exhibits spatial correlations. The underlying key principle for all of them is that a network should predict the value of a given pixel in the denoised image without directly observing its noisy counterpart, hence the term *blind-spot*. Therefore, the network can only learn from the neighboring pixels, which — under the assumption of independent noise — do not carry any information about the noise affecting the target pixel, thus preventing the network from predicting a noisy image.

Krull et al. first introduce this concept in their Noise2Void (N2V) paper [10]. The authors consider training a network to predict the center pixel of a single patch of the input image in a supervised fashion, using the actual pixel value as the target. To prevent the network from simply learning the identity, they propose restricting the output pixel’s receptive field by masking the center pixel. The receptive field refers to the set of pixels in the input that influences a particular pixel in the output, as visualized in Figure 3.1. However, this process is not feasible in practice, as a whole patch has to be processed to obtain a single output pixel. In order to allow efficient training, they approximate this behavior by training on random patches, for each of which a fixed number of pixels are randomly replaced by local neighbors, using their respective original noisy values as targets.

In Noise2Self (N2S) [2], Batson et al. generalize this concept to sets of variables, instead of single pixels only, by introducing the notion of  $\mathcal{J}$ -invariance. For a noisy input image  $y \in \mathbb{R}^m$ , let  $\mathcal{J}$  be a partition of the dimensions  $\{1, \dots, m\}$ . For a subset of the dimensions  $J \in \mathcal{J}$ ,  $x_J$  denotes  $x$  restricted to the dimensions  $J$ . A function  $f : \mathbb{R}^m \rightarrow \mathbb{R}^m$  is said to be  $\mathcal{J}$ -invariant if, for each  $J \in \mathcal{J}$ ,  $f(x)_J$  does not depend on  $x_J$ , i.e.,

$$f(x)_J = f(x_{J^c})_J, \quad (3.3)$$

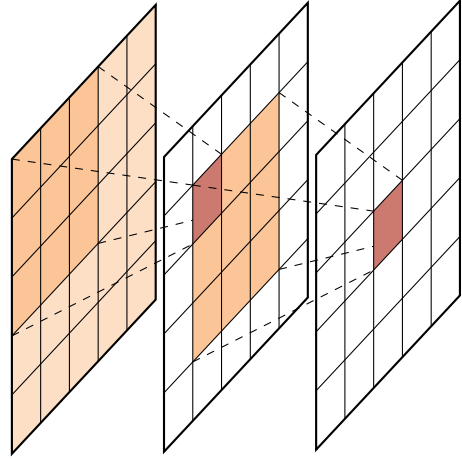


**Figure 3.1:** Receptive field in CNNs, using a  $3 \times 3$  kernel.

where  $J^c$  refers to the complement of  $J$ . The training objective from (3.1) then becomes

$$\operatorname{argmin}_{\theta} \sum_{i=1}^n \|f_{\theta}(y_{J^c}^i)_J - y_J^i\|_2^2. \quad (3.4)$$

As in N2V,  $x_{J^c}$  is obtained through a masking strategy; the main difference lies in the way the masked pixels are replaced. While N2S directly uses random values, N2V chooses the replacement pixels randomly from local neighbors.

Laine et al. [11] choose a different approach; instead of relying on masking strategies, they directly manipulate the receptive field by adapting the network architecture itself. In Noise2Same [30], the authors demonstrate that, in practice, both N2V and N2S are not strictly  $\mathcal{J}$ -invariant and thus conclude that strict  $\mathcal{J}$ -invariance is not necessary for achieving good denoising performance. Therefore, they propose to do without explicit manipulation of the receptive field and instead add a regularization term that encourages the network to learn an approximately  $\mathcal{J}$ -invariant mapping by itself.

# Chapter 4

## Methods

While the self-supervised denoising methods discussed so far eliminate the need for clean data, most still require large datasets of noisy images or are limited to specific noise types. A notable exception is the Deep Image Prior (DIP) introduced by Ulyanov et al. [25]. DIP is a zero-shot method, meaning it operates on a single noisy sample, and does not make any explicit assumptions about the noise distribution.

In this chapter, we present DIP and its various extensions. First, we describe the fundamental principles of DIP, followed by common techniques used to further regularize the solution. Finally, we explore additional DIP-based approaches that build upon these foundations.

### 4.1 Deep Image Prior

As discussed in Section 2.1, denoising is an ill-posed inverse problem and therefore appropriate regularization is crucial in order to obtain plausible solutions. This is typically expressed as an optimization problem of the form

$$\hat{x} = \operatorname{argmin}_x L(x, y) + R(x), \quad (4.1)$$

where  $L(x, y)$  is a data fidelity term that ensures that the denoised estimate  $\hat{x}$  stays close to the noisy signal  $y$  and  $R(x)$  is the regularizer. Most traditional, non-deep-learning methods, such as total variation denoising [21], rely on an explicit regularization term. The self-supervised methods discussed in Section 3.2 do not necessarily include such a term; however, they do make specific assumptions about the solution (e.g., zero-mean or spatially independent noise), which are implicitly encoded in the training procedure — through techniques like sub-sampling or masking.

In contrast, DIP does not make any explicit assumptions about the noise or image structure. Instead, it relies solely on the architecture of a convolutional neural network to implicitly regularize the solution. The key idea is to parameterize an image  $x$  as the output of an CNN  $f_\theta$  through  $x = f_\theta(z)$ , where  $z$  refers to a random vector, e.g.,  $z \sim \mathcal{N}(\mathbf{0}, \sigma^2 \mathbf{I})$ .

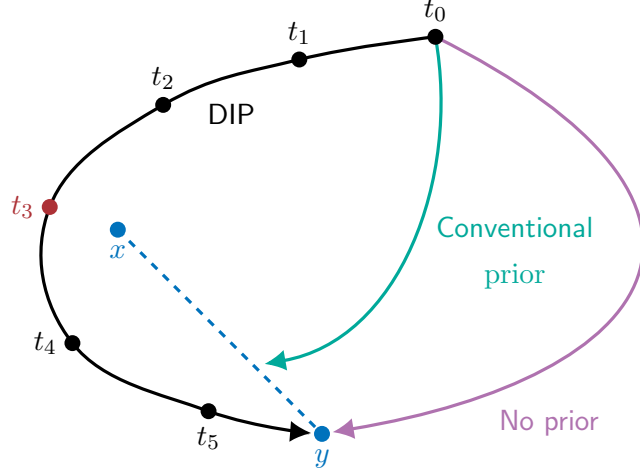


**Figure 4.1:** The effect of priors. Without regularization, the optimization leads directly to the noisy image  $y$ . Conventional priors shift the solution closer to the clean image  $x$ . DIP will eventually overfit to  $y$ , but often the optimization path will pass close to  $x$ , with the optimal stopping point marked in red. Figure adapted from [25].

This means that instead of optimizing  $x$  directly, the reconstruction is constrained by the network’s ability to map  $z$  to a plausible image. In terms of (4.1), the MSE is used as the loss function and the regularizer  $R(x)$  is replaced with the implicit prior induced by the network structure, leading to the following optimization:

$$\theta^* = \operatorname{argmin}_{\theta} \|f_{\theta}(z) - y\|_2^2. \quad (4.2)$$

After training the network using gradient descent, the denoised estimate is then obtained as  $\hat{x} = f_{\theta^*}(z)$ . The random vector  $z$  remains fixed throughout the training process. The regularizing effect of this parametrization relies on the observation that CNNs tend to capture structured patterns (e.g., edges and textures) before fitting to high-frequency noise. However, since the network is sufficiently expressive, it will eventually memorize the noise, leading to overfitting. Thus, it is crucial to identify the optimal stopping point, at which the network successfully learned the underlying image structure while minimizing the influence of noise. This process is visualized in Figure 4.1. Formally, this regularizer can be expressed as

$$R(x) = \begin{cases} 0 & f_{\theta} \text{ can produce } x \text{ in } N \text{ steps} \\ +\infty & \text{else} \end{cases} \quad (4.3)$$

where  $N$  refers to a fixed maximum number of iterations. However, such a fixed stopping point is not ideal because the optimal stopping point depends on factors such as the specific image  $x$ , the random vector  $z$  and also the initial network parameters  $\theta_0$ .

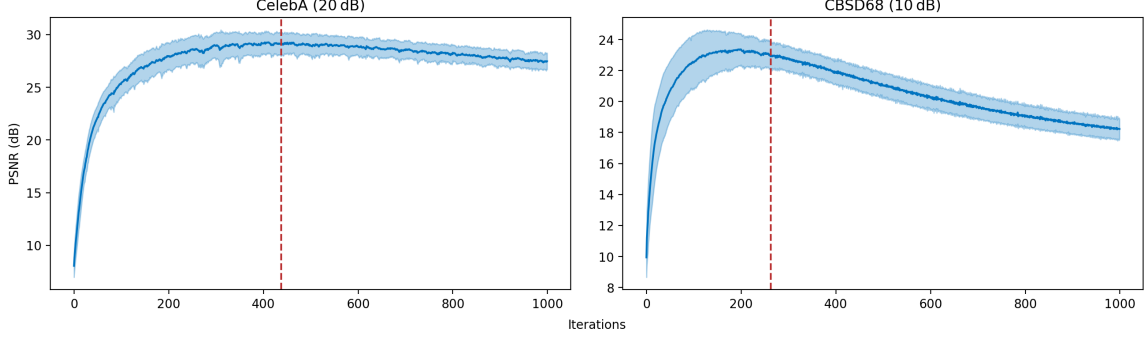


**Figure 4.2:** ES-WMV on different datasets and noise levels. Image quality is evaluated on 20 random images from the CelebA (left) and CBSD68 (right) datasets, with Gaussian noise added at levels specified in the titles. The blue line represents the mean PSNR, the light blue shaded area indicates  $\pm 1$  standard deviation. The red line marks the average detected stopping point.

#### 4.1.1 Early Stopping

The process of halting the training to mitigate overfitting is known as early stopping (ES). As discussed earlier, a fixed stopping point generally will not work well. Therefore, we need to find a way to dynamically detect optimal stopping points during training. In principle, if the clean ground-truth image  $x$  were available, this would be trivial: One could simply track image quality using an appropriate metric, e.g., PSNR or SSIM, and stop training at its peak. However, since  $x$  is inherently unknown in the denoising setting, we need an alternative criterion to determine when to stop.

Wang et al. [28] propose such a criterion based on the running variance of the DIP reconstructions over time. Let  $\{x^t\}_{t \geq 1}$  denote the sequence of the respective denoised estimates  $x^t = f_{\theta^t}(z)$  at iteration  $t$ . The authors observe that the MSE  $\|x^t - x\|_F^2$  initially drops as the networks learns the image structure, and then rises again due to overfitting to noise, leading to a U-shaped curve. However, once again,  $x$  is unknown in practice, so the goal is to detect the minimum of said curve without access to  $x$ . To achieve this, they consider the running variance over a window of  $W$  iterations, given by

$$\text{Var}(t) = \frac{1}{W} \sum_{w=0}^{W-1} \left\| x^{t+w} - \frac{1}{W} \sum_{i=0}^{W-1} x^{t+i} \right\|_F^2. \quad (4.4)$$

Intuitively, when  $t$  is near the optimal stopping point, all  $x^{t,i}$ s should be close to  $x$ , leading to  $\frac{1}{W} \sum_{w=0}^{W-1} x^{t+w} \approx x$ . Plugging this back into (4.4), we see that when  $t$  is near the optimum,  $\text{Var}(t)$  approximates the average MSE across the window. Therefore, they propose using the minimum of the variance curve to determine the stopping point. To improve robustness, they introduce a patience parameter  $P$ , allowing the variance to stagnate for up to  $P$  iterations before stopping. This approach, termed early stopping via windowed moving variance (ES-WMV), is effective across different noise levels and types of images, as demonstrated in Figure 4.2.

### 4.1.2 Total Variation

Another way to prevent overfitting is to incorporate an additional explicit regularization term, such as total variation (TV) [21]. TV encourages piecewise smoothness by penalizing abrupt intensity changes in the image. Formally, for an image  $x \in \mathbb{R}^{m \times n}$ , it is defined as

$$\text{TV}(x) = \sum_{i=1}^{m-1} \sum_{j=1}^{n-1} (|x_{i+1,j} - x_{i,j}| + |x_{i,j+1} - x_{i,j}|). \quad (4.5)$$

Liu et al. propose combining the implicit network regularization of DIP with an explicit TV regularizer, leading to the method known as DIP-TV [16]. This results in the following optimization problem:

$$\theta^* = \underset{\theta}{\operatorname{argmin}} \|f_{\theta}(z) - y\|_2^2 + \lambda \text{TV}(f_{\theta}(z)). \quad (4.6)$$

## 4.2 Deep Diffusion Image Prior

## 4.3 Self-Guided Deep Image Prior

## Chapter 5

# Results





## Chapter 6

# Discussion



## Chapter 7

## Conclusion



# Bibliography

- [1] Jimmy Lei Ba, Jamie Ryan Kiros, and Geoffrey E. Hinton. *Layer Normalization*. 2016. arXiv: 1607.06450 [stat.ML]. URL: <https://arxiv.org/abs/1607.06450>.
- [2] Joshua Batson and Loic Royer. “Noise2Self: Blind Denoising by Self-Supervision”. In: *Proceedings of the 36th International Conference on Machine Learning*. Ed. by Kamalika Chaudhuri and Ruslan Salakhutdinov. Vol. 97. Proceedings of Machine Learning Research. PMLR, Sept. 2019, pp. 524–533. URL: <https://proceedings.mlr.press/v97/batson19a.html>.
- [3] Yangkang Chen et al. “Denoising of Distributed Acoustic Sensing Seismic Data Using an Integrated Framework”. In: *Seismological Research Letters* 94.1 (Nov. 2022), pp. 457–472.
- [4] Tim Dean, T. Cuny, and Arthur Hartog. “Determination of the Optimum Gauge Length for Borehole Seismic Surveys Acquired Using Distributed Vibration Sensing”. In: June 2015. DOI: 10.3997/2214-4609.201412740.
- [5] Ian Goodfellow, Yoshua Bengio, and Aaron Courville. *Deep Learning*. <http://www.deeplearningbook.org>. MIT Press, 2016.
- [6] Arthur H. Hartog. *An Introduction to Distributed Optical Fibre Sensors*. CRC Press, 2017. URL: <http://dx.doi.org/10.1201/9781315119014>.
- [7] Jie Hu et al. *Squeeze-and-Excitation Networks*. 2019. arXiv: 1709.01507 [cs.CV]. URL: <https://arxiv.org/abs/1709.01507>.
- [8] Tao Huang et al. “Neighbor2Neighbor: Self-Supervised Denoising From Single Noisy Images”. In: *Proceedings of the IEEE/CVF Conference on Computer Vision and Pattern Recognition (CVPR)*. June 2021, pp. 14781–14790.
- [9] Sergey Ioffe and Christian Szegedy. “Batch Normalization: Accelerating Deep Network Training by Reducing Internal Covariate Shift”. In: *CoRR* abs/1502.03167 (2015). arXiv: 1502.03167. URL: <http://arxiv.org/abs/1502.03167>.
- [10] Alexander Krull, Tim-Oliver Buchholz, and Florian Jug. “Noise2Void - Learning Denoising From Single Noisy Images”. In: *2019 IEEE/CVF Conference on Computer Vision and Pattern Recognition (CVPR)*. 2019, pp. 2124–2132. DOI: 10.1109/CVPR.2019.00223.

- [11] Samuli Laine et al. “High-Quality Self-Supervised Deep Image Denoising”. In: *Advances in Neural Information Processing Systems*. Ed. by H. Wallach et al. Vol. 32. Curran Associates, Inc., 2019. URL: [https://proceedings.neurips.cc/paper\\_files/paper/2019/file/2119b8d43eafcf353e07d7cb5554170b-Paper.pdf](https://proceedings.neurips.cc/paper_files/paper/2019/file/2119b8d43eafcf353e07d7cb5554170b-Paper.pdf).
- [12] S Lapins et al. “DAS-N2N: machine learning distributed acoustic sensing (DAS) signal denoising without clean data”. In: *Geophysical Journal International* 236.2 (Nov. 2023), pp. 1026–1041. ISSN: 1365-246X. DOI: 10.1093/gji/ggad460. URL: <http://dx.doi.org/10.1093/gji/ggad460>.
- [13] Y. LeCun et al. “Backpropagation Applied to Handwritten Zip Code Recognition”. In: *Neural Computation* 1.4 (1989), pp. 541–551. DOI: 10.1162/neco.1989.1.4.541.
- [14] Jaakko Lehtinen et al. “Noise2Noise: Learning Image Restoration without Clean Data”. In: *Proceedings of the 35th International Conference on Machine Learning*. Ed. by Jennifer Dy and Andreas Krause. Vol. 80. Proceedings of Machine Learning Research. PMLR, Oct. 2018, pp. 2965–2974. URL: <https://proceedings.mlr.press/v80/lehtinen18a.html>.
- [15] A. Lellouch et al. “Low-Magnitude Seismicity With a Downhole Distributed Acoustic Sensing Array—Examples From the FORGE Geothermal Experiment”. In: *Journal of Geophysical Research: Solid Earth* 126.1 (Dec. 2020). ISSN: 2169-9356. DOI: 10.1029/2020jb020462. URL: <http://dx.doi.org/10.1029/2020JB020462>.
- [16] Jiaming Liu et al. “Image Restoration Using Total Variation Regularized Deep Image Prior”. In: *ICASSP 2019 - 2019 IEEE International Conference on Acoustics, Speech and Signal Processing (ICASSP)*. 2019, pp. 7715–7719. DOI: 10.1109/ICASSP.2019.8682856.
- [17] Youssef Mansour and Reinhard Heckel. “Zero-Shot Noise2Noise: Efficient Image Denoising without any Data”. In: *2023 IEEE/CVF Conference on Computer Vision and Pattern Recognition (CVPR)*. 2023, pp. 14018–14027. DOI: 10.1109/CVPR52729.2023.01347.
- [18] Meghan S. Miller, John Townend, and Voon Hui Lai. “The South Island Seismology at the Speed of Light Experiment (SISSLE): Distributed Acoustic Sensing Across and Along the Alpine Fault, South Westland, New Zealand”. In: *Seismological Research Letters* (Dec. 2024). ISSN: 0895-0695. DOI: 10.1785/0220240322. eprint: <https://pubs.geoscienceworld.org/ssa/srl/article-pdf/doi/10.1785/0220240322/7068598/srl-2024322.1.pdf>. URL: <https://doi.org/10.1785/0220240322>.
- [19] Nick Moran et al. “Noisier2Noise: Learning to Denoise From Unpaired Noisy Data”. In: *Proceedings of the IEEE/CVF Conference on Computer Vision and Pattern Recognition (CVPR)*. June 2020.

- [20] Zhaoyang Niu, Guoqiang Zhong, and Hui Yu. “A review on the attention mechanism of deep learning”. In: *Neurocomputing* 452 (2021), pp. 48–62. ISSN: 0925-2312. DOI: <https://doi.org/10.1016/j.neucom.2021.03.091>. URL: <https://www.sciencedirect.com/science/article/pii/S092523122100477X>.
- [21] Leonid I. Rudin, Stanley Osher, and Emad Fatemi. “Nonlinear total variation based noise removal algorithms”. In: *Physica D: Nonlinear Phenomena* 60.1 (1992), pp. 259–268. ISSN: 0167-2789. DOI: [https://doi.org/10.1016/0167-2789\(92\)90242-F](https://doi.org/10.1016/0167-2789(92)90242-F). URL: <https://www.sciencedirect.com/science/article/pii/016727899290242F>.
- [22] David E. Rumelhart, Geoffrey E. Hinton, and Ronald J. Williams. “Learning representations by back-propagating errors”. In: *Nature* 323 (Oct. 1986), pp. 533–. URL: <http://dx.doi.org/10.1038/323533a0>.
- [23] Irwin Sobel. “An Isotropic 3x3 Image Gradient Operator”. In: *Presentation at Stanford AI Lab (SAIL)* (1968).
- [24] “TODO”. In: ().
- [25] Dmitry Ulyanov, Andrea Vedaldi, and Victor Lempitsky. “Deep Image Prior”. In: *International Journal of Computer Vision* 128.7 (Mar. 2020), pp. 1867–1888. ISSN: 1573-1405. DOI: 10.1007/s11263-020-01303-4. URL: <http://dx.doi.org/10.1007/s11263-020-01303-4>.
- [26] Dmitry Ulyanov, Andrea Vedaldi, and Victor S. Lempitsky. “Instance Normalization: The Missing Ingredient for Fast Stylization”. In: *CoRR* abs/1607.08022 (2016). arXiv: 1607.08022. URL: <http://arxiv.org/abs/1607.08022>.
- [27] Ashish Vaswani et al. *Attention Is All You Need*. 2023. arXiv: 1706.03762 [cs.CL]. URL: <https://arxiv.org/abs/1706.03762>.
- [28] Hengkang Wang et al. “Early Stopping for Deep Image Prior”. In: *Transactions on Machine Learning Research* (2023). ISSN: 2835-8856. URL: <https://openreview.net/forum?id=231ZzrLC8X>.
- [29] Yuxin Wu and Kaiming He. “Group Normalization”. In: *CoRR* abs/1803.08494 (2018). arXiv: 1803.08494. URL: <http://arxiv.org/abs/1803.08494>.
- [30] Yaochen Xie, Zhengyang Wang, and Shuiwang Ji. “Noise2Same: Optimizing A Self-Supervised Bound for Image Denoising”. In: *Advances in Neural Information Processing Systems*. Ed. by H. Larochelle et al. Vol. 33. Curran Associates, Inc., 2020, pp. 20320–20330. URL: [https://proceedings.neurips.cc/paper\\_files/paper/2020/file/ea6b2efbdd4255a9f1b3bbc6399b58f4-Paper.pdf](https://proceedings.neurips.cc/paper_files/paper/2020/file/ea6b2efbdd4255a9f1b3bbc6399b58f4-Paper.pdf).
- [31] Dan Zhang et al. *Unleashing the Power of Self-Supervised Image Denoising: A Comprehensive Review*. 2024. arXiv: 2308.00247 [eess.IV]. URL: <https://arxiv.org/abs/2308.00247>.

- [32] Kai Zhang et al. “Beyond a Gaussian Denoiser: Residual Learning of Deep CNN for Image Denoising”. In: *IEEE Transactions on Image Processing* 26.7 (July 2017), pp. 3142–3155. ISSN: 1941-0042. DOI: 10.1109/tip.2017.2662206. URL: <http://dx.doi.org/10.1109/TIP.2017.2662206>.



# Appendix A

## Supplementary Information

### A.1 Acronyms

---

<b>CNN</b>	convolutional neural network
<b>DAS</b>	distributed acoustic sensing
<b>DIP</b>	deep image prior
<b>MSE</b>	mean squared error
<b>PSNR</b>	peak signal-to-noise ratio
<b>SSIM</b>	structural similarity index measure

---

**Table A.1:** List of common acronyms.